

Developing a new interatomic potential for U-Mo-Xe by using an Ab initio force-matching method

D. Smirnova, Z. Insepov, J. Rest, A.M. Yacout¹
Argonne National Laboratory, Illinois, USA

S. Starikov, A. Kuxin, V. Stegailov, G. Norman
Joint Institute for High Temperature of RAS, Moscow, Russia.

Abstract

A new embedded-atom method (EAM) potential for a U-Mo-Xe system has been developed by using an Ab initio force-matching calculation method. Specifically, the new potential was built by using 121 reference structures for liquid uranium and molybdenum, solid alpha- and gamma-uranium, solid bcc molybdenum, pure xenon, and corresponding binary and ternary systems for a wide range of temperatures and pressure. The values of the lattice constants, thermal expansion coefficients, and P-T and P-V curves of uranium showed good agreement with experiment and density functional theory (DFT) Ab initio calculations. Calculated energies of point defects in pure molybdenum were comparable to those obtained with a Xe-Mo EAM potential and DFT calculations. However, the energy of vacancy formation in pure γ -U showed worse agreement with the experimental value.

Introduction

The development of prospective low-enriched nuclear fuel based on uranium alloys has become more important because of worldwide efforts encouraging the development of low-enriched ²³⁵U fuels [1]. The main incentive is to reduce the danger of using the nuclear fuels by developing new fuel material that is safer and more effective. According to experimental data, low-enriched uranium and uranium-molybdenum alloys have good strength and stainless properties [2–4]. Therefore the UxMo alloys can be considered as new prospective fuel alloys. However, the key problem hindering the use of the new uranium alloys in industry is the stability of the fuel against defect formation, swelling, and phase transitions caused by heating and irradiation by fission products. Additionally, fuel irradiation leads to formation of nanoscale structures, including voids and bubbles filled with xenon gas [5]. These structural changes significantly influence the mechanical and thermal properties of the fuel and eventually lead to destruction of the fuel cell and, hence, to a decrease in its endurance period.

Molecular dynamics (MD) is a powerful tool for studying the structure changes in the material and for analyzing the corresponding changes in the material's properties. Specifically, MD studies have helped researchers obtain a better understanding of the mechanisms of the structural changes occurring in U-Mo alloys; indeed, in some cases of high temperature and pressure, MD has proved to be the only feasible method of revealing the physics of the materials. The interatomic potentials were the key property of the atomistic MD and the biggest task in initiation of the simulation study of the new fuel material.

¹ Corresponding author: yacout@anl.gov

Presented here is the first attempt to develop a new interatomic potential for the U-Mo-Xe system, since a potential for uranium-molybdenum-xenon system does not exist. The new potential will allow scientists to calculate the thermodynamical and mechanical properties of uranium-molybdenum alloys and can be applied to study the mechanisms of formation and evolution of the radiation defects. The potential is built based on the concept of the embedded-atom model [6] using a force-matching method [7]. The calculated ab initio values of forces per atom, energies, and stresses were used as reference data during the optimization of the potential functions. The potential was used to calculate the properties of the fuel alloys (containing from 6 to 10 weight percent of molybdenum) and pure phases of uranium and molybdenum. The goal of the present work is to study in detail the mechanisms of the atomistic structure and properties changes occurring in the U-Mo fuel alloys under heating and irradiation.

Computational model

An Ab initio force-matching method (FMM), originally proposed by Ercolessi and Adams [7], was used in all our calculations. The method is suitable for developing an accurate interatomic potential for a ternary uranium-molybdenum-xenon system. FMM allows development of the interatomic potentials for complex systems and applicable for multielemental and multiphase alloy systems. FMM was successfully applied to constructing of an interatomic potential for a Mo-Xe system [8] and pure U [9]. The procedure of construction is as follows.

At the first stage, the reference database of the lattice structures is built. This reference database contains values of the atomic forces, energies and stresses calculated within the DFT ab initio methods for some reference atomic structures representing pure uranium, pure molybdenum, and xenon and also for complex structures: U-Mo, Mo-Xe and U-Mo-Xe systems under various pressure-temperature conditions. Composition of the binary and ternary systems was also varied in an interval of atomic weights of Mo from several percent to almost 20%.

At the second stage, the embedded-atom-method potential is optimized. During the optimization one must minimize the deviations between the reference values and the calculated values obtained with the developed force-matched potential and, consequently, find a potential that reproduces the reference data with the best accuracy. In what follows we describe both parts of the procedure in more detail.

Construction of the reference database

For computing the reference database, a set of configurations was created containing the information about the atomic coordinates for the systems with a small number of atoms. A full set of configurations previously built for developing the potentials for Mo-Xe system [8] and for pure uranium [9] was used and additional configurations representing binary U-Mo and ternary U-Mo-Xe systems were built. Specifically, the area of Mo concentration from 6 to 20 at. % was studied, because this composition corresponded to the most realistic composition of future U-Mo fuel alloys.

A list of all 19 additional configurations is presented below.

List of the reference structures representing U-Mo alloys with/without Xe

1. 128 atoms: 112 U atoms, 16 Mo atoms (12.5 at. % Mo).

- T ~ 1000 K, liquid U-Mo alloy without Xe
 2. 128 atoms: 120 U atoms, 8 Mo atoms (6.2 at. % Mo).
 T ~ 1050 K, liquid U-Mo alloy without Xe
 3. 128 atoms: 112 U atoms, 16 Mo atoms (12.5 at. % Mo).
 T ~ 1150 K, liquid U-Mo alloy without Xe
 4. 128 atoms: 112 U atoms, 16 Mo atoms (12.5 at. % Mo).
 T ~ 1200 K, liquid U-Mo alloy without Xe
 5. 128 atoms: 112 U atoms, 16 Mo atoms (12.5 at. % Mo).
 T ~ 400 K, crystal bcc structure, without Xe
 6. 128 atoms: 120 U atoms, 8 Mo atoms (6.2 at. % Mo).
 T ~ 350 K, crystal bcc structure, without Xe
 7. 128 atoms: 112 U atoms, 16 Mo atoms (12.5 at. % Mo).
 T ~ 270 K, crystal bcc structure, without Xe (the arrangement of Mo atoms differs from the one in conf. (5))
 8. 128 atoms: 104 U atoms, 24 Mo atoms (18.75 at. % Mo)
 T ~ 270 K, crystal bcc structure, without Xe
 9. 128 atoms: 112 U atoms, 16 Mo atoms (12.5 at. % Mo).
 T ~ 360 K, crystal bcc structure, slightly expanded (lattice parameter a is 3.48 Å instead of the equilibrium 3.441 Å), without Xe
 10. 128 atoms: 112 U atoms, 16 Mo atoms (12.5 at. % Mo).
 T ~ 400 K, crystal bcc structure, slightly compressed (a is 3.42 Å instead of the equilibrium value 3.441 Å), without Xe
 11. 129 atoms: 104 U, 24 Mo 1Xe (18.75 at. % Mo). T ~ 300 K, crystal bcc structure. The single Xe atom originally is embedded as an interstitial in octahedral pore. But then during the calculation it relaxes to the lattice site, knocking out one U atom and causing the single interstitial U atom formation.
 12. 129 atoms: 112 U, 16 Mo, 1 Xe (12.5 at. % Mo). T ~ 300 K, crystal bcc structure. The single Xe atom originally is embedded as an interstitial in tetrahedral pore but also relaxes to the lattice site, knocking out a single U atom.
 13. 128 atoms: 104 U, 23 Mo, 1 U (18 at. % Mo). T ~ 300 K, crystal bcc structure. The single Mo atom in the lattice site is replaced by the single Xe atom.
 14. 128 atoms: 110 U, 2 Mo, 16 Xe, T ~ 300 K, crystal bcc structure.
 15. 128 atoms: 110 U, 2 Mo, 16 Xe, T ~ 300 K, crystal bcc structure. The arrangement of the Xe atoms differs from the one selected in (14).
 16. 128 atoms: 104 U, 24 Mo, T ~ 450 K, crystal bcc structure. Lattice parameter equals 3.35346 Å, compressed configuration.
 17. 128 atoms: 104 U, 24 Mo, T ~ 450 K, crystal bcc structure. Lattice parameter equals 3.285 Å, compressed configuration.
 18. 128 atoms: 104 U, 24 Mo, T ~ 450 K, crystal bcc structure. Lattice parameter equals 3.21658 Å, compressed configuration.
 19. 128 atoms: 104 U, 24 Mo, T ~ 460 K, crystal bcc structure. Lattice parameter equals 3.148148 Å, compressed configuration.

In order to obtain thermal displacements in all reference structures, short (~picosecond) MD computations were carried out with the trial potential constructed from the potentials for U and

Mo-Xe systems. The final atomic arrangement obtained after the MD calculation for a single structure was one of the required configurations. All MD calculations in this work were performed with the LAMMPS code [10]. The simulation box with periodic boundary conditions in all three dimensions contains 128/129 atoms (depending on the simulated structure; see the list above).

Next, the DFT ab initio calculations of the reference forces, energies per atom, and the stress tensors for each configuration were performed. The plane-wave program code VASP was used [11]. In order to represent the inner electronic structure of uranium, projector augmented-wave pseudo-potentials were adapted that had been developed by Kresse and Joubert [12] and implemented in the VASP package. The basis plane-wave energy cutoff was set at 450 eV. Based on the symmetry of the studied structures, a set of k-points meshes— $2 \times 2 \times 2$ for bcc U-Mo and U-Mo-Xe—was chosen. These values provided the convergence of energies. The reference database contained information about pure components of the U-Mo-Xe system and the additional binary and ternary systems and consisted of 17,926 values of the atomic forces (or 53,778 force components), 137 values of the energy per atom, and 802 components of the stress tensor.

Optimization of the potential functions

For the U-Mo-Xe system the set of the potential functions was chosen within the frame of the embedded-atom method [6], allowing us to take into account many-body interatomic interactions:

$$U = \sum_{i < j} \varphi(r_{ij}) + \sum_j F(\bar{\rho}_j), \quad (1)$$

$$\bar{\rho}_j = \sum_{i \neq j} \rho(r_{ij}), \quad (2)$$

where the first term in expression (1) represents the pair interaction, and the second term depending on the effective electronic density (2) allows us to consider many-body interatomic interactions taking place in metals.

To describe the potential for ternary system within the frame of the embedded-atom method, we must determine 12 functions:

- 6 functions describing possible pair interactions between U and U, U and Mo, U and Xe, Mo and Mo, Mo and Xe, Xe and Xe
- 3 functions for electron density: ρ (U), ρ (Mo), ρ (Xe)
- 3 embedded functions: F (U), F (Mo), F (Xe).

In order to construct an EAM potential using the force-matching method, one must select a certain number of trial functions (as a set of cubic spline knots that uniquely define the whole potential) and calculate the forces, energies, and stresses with this given potential. In our simulations, 12 trial potential functions were chosen. Then the calculated values were compared with the reference ab initio data by calculation of the target function (3):

$$Z_F = \sum_{j=1}^{N_A} \sum_{\alpha=x,y,z} W_j \frac{(f_{j\alpha} - f_{0,j\alpha})^2}{f_{0,j}^2 + \epsilon_j}, \quad (3)$$

where f_j is calculated force, $f_{0,j}$ is reference force, W_j is computational weight assigned to an atom j , and ϵ_j equals 0.1 (eV/\AA)^2

If a trial potential did not give good agreement with the reference data, the trial functions were automatically changed to minimize the target function and, hence, to minimize the difference between reference data and calculated ones. The optimizing iterations were conducted with the *potfit* [13] code, with the multidimensional minimization carried out in a large parameter space. The number of parameters was equal to the number of the spline knots. For the 12 functions describing the U-Mo-Xe system, the number of parameters was about 200 (depending on a chosen number of cubic spline knots).

Verification of the potentials obtained

After the *potfit* code execution, the generated potential was verified by test MD calculations of the properties of U-Mo-Xe system and its components.

According to the literature sources, U-Mo alloys have been experimentally studied for many years, and significant information exists about their behavior under irradiation, lattice parameters, heat capacity, thermal expansion, electrical resistance, density, thermal conductivity, and melting temperature [1–5]. Some of the data (for example, lattice constants and thermal expansion) was useful for the first step of the verification because it was easily computed and the results helped us understand whether the potential was able to reproduce U-Mo alloys. Also, the potential was applied for calculating the properties of pure components of the system (U, Mo, and Xe) to test their repeatability.

We built four versions of the U-Mo-Xe potential, improving, from version to version, the ability to represent the system studied.

Calculations of the lattice constants

As the first basic step during verification we calculated the lattice parameters of uranium, molybdenum, and U-Mo alloys. Specifically, we performed LAMMPS [10] MD calculations with the full set of developed potentials. For these computations we varied the lattice constants of the given structures at the given temperatures to obtain zero pressure in the system and to exclude possible deviations between the pressure components. Using each of the potential versions, we found the corresponding lattice constants that give $P_{xx} = P_{yy} = P_{zz} = P \sim 0 \text{ GPa}$ for each phase studied. The results are summarized in Table 1.

Table 1 – Lattice constants (Å) of U-Mo alloys and pure U and Mo in comparison with the experimental data

	Experiment [3, 14,15]	U-Mo-Xe 1.0	U-Mo-Xe 1.2	U-Mo-Xe 1.3	U-Mo-Xe 1.4
U-6Mo , 300 K	3.44155	3.5575 3 %	3.4705 0.8 %	3.462 0.6 %	3.467 0.7 %
U-10Mo , 300 K	3.4219	3.549 3.7 %	3.426 0.1 %	3.4183 0.1 %	3.4183 0.1 %
α-U , 300 K					
<i>a</i>	2.8537	2.85671 0.1 %	2.86983 0.5 %	2.85394 0 %	2.8539 0 %
<i>b</i>	5.8695	5.76632 1.7 %	5.76142 1.8 %	5.75155 2%	5.7515 2 %
<i>c</i>	4.9548	4.93164 0.5 %	4.93248 0.4 %	4.94288 0 %	4.9428 0.2 %
<i>y</i>	0.1025	0.1015 0.1 %	0.1015 0.1 %	0.1025 0 %	0.1025 0 %
γ-U , ~ 1100 K	3.557	3.59 0.9 %	3.532 0.7 %	3.543 -0.4 %	3.542 -0.4 %
Mo , ~ 0 K	3.1472	3.1518 0.2 %	3.1517 0.2 %	3.1469 0 %	3.1474 0 %

Also, it is possible to calculate the changes of the lattice constants of U-10Mo with the temperature. The computations of the lattice constants in this case were carried out in the same way as described above. Results obtained for all four versions of the potentials are compared in Fig. 1. According to this data, the thermal expansion provided with the potential 1.4 is approximately two times lower than the experimental value [3].

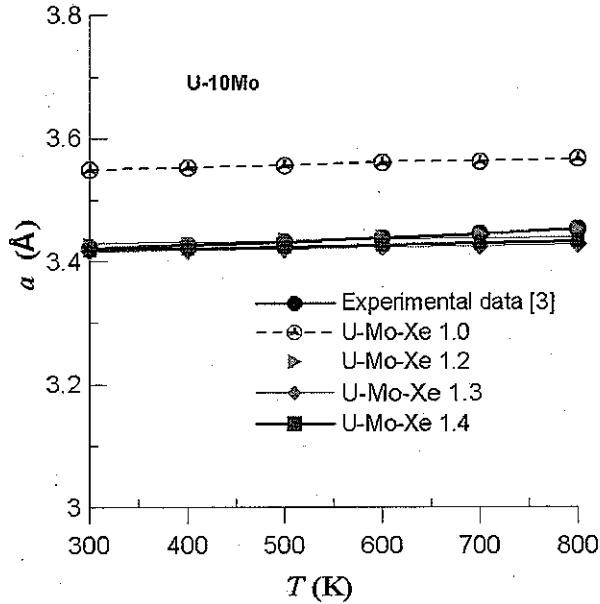


Figure 1 – Lattice parameter of U-10Mo in comparison with the data [3]. The deviation between the values for the 800 K point is about 0.5%.

We also calculated the pressure-temperature dependence at the given volume for α -U. Models of α -U were built with the given lattice constants (see Table 1; we use the values that gives $P \sim 0$ GPa for each potential). Then the volume of each model ($V = V_{eq}(300 \text{ K})$) was fixed, the temperature was changed, and the corresponding pressure values were calculated for each temperature point.

Figure 2 shows that the potentials 1.3 and 1.4 overestimates the pressure values, but the dependence is in agreement with the experimental data [16].

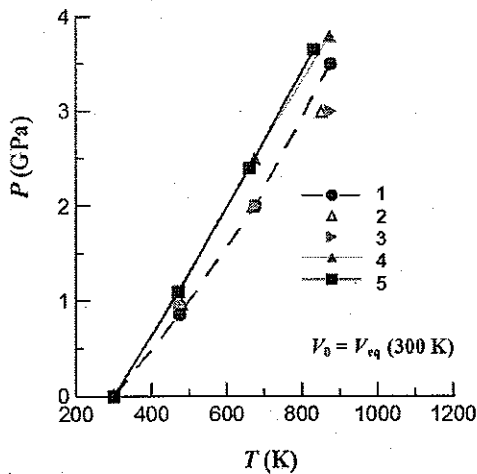


Figure 2 – Pressure-temperature dependence calculated for α -U at the given constant volume. 1 – Experimental data [16]; 2 – results obtained with EAM potential for pure U [9]; 3 – potential U-Mo-Xe 1.2; 4 – potential U-Mo-Xe 1.3; 5 – potential U-Mo-Xe 1.4.

One can see from Figures 1 and 2 that potential 1.2 gives the better performance while representing thermal expansion of pure uranium and of U-10Mo. It also was found that this version of the potential cannot be applied for examining pure uranium phases because it does not describe the mechanical properties (bulk modulus and elastic constants) of pure uranium with good accuracy.

Bulk modulus of α -U

Bulk modulus was determined from MD simulations of uniform compression and expansion of the equilibrium volume as

$$B = -V_{eq} \frac{\Delta P}{\Delta V}, \tag{4}$$

where V_{eq} is the equilibrium phase volume and ΔV is about 2%.

The corresponding results for the bulk modulus are summarized in Table 2.

Hence, the potential version 1.2 was improved to get potentials 1.3 and, then, 1.4 that represent the elastic properties of the pure components with better accuracy.

From this point, verification of the last version, 1.4, was undertaken in order to understand how it works in various cases for U-Mo and pure U, Mo, and Xe.

Table 2 – Bulk modulus of the α -U at 300 K calculated with the four versions of the potential, in comparison with the experimental data [17]

Experiment [17]	135.5 GPa
B (ver 1.0), 300 K	185 GPa
B (ver 1.2), 300 K	180 GPa
B (ver 1.3), 300 K	107 GPa
B (ver 1.4), 300 K	107 GPa

Elastic constants for pure U and Mo

The elastic constants for pure α - and γ -uranium were calculated and compared with the existing experimental data. The results of comparison are given in Table 3.

The elastic constants c_{ij} were calculated from MD-simulation of uniaxial compression of solid phases (U and Mo). The elastic constants can be determined as follows (in Voigt notation):

$$c_{ij} = \frac{\Delta P_{jj}}{\varepsilon_{ii}}, \quad (5)$$

where ΔP_{jj} is the change in pressure along the axis j providing that the model size l_i^0 is reliably decreased along one of its dimensions and the corresponding deformation equals

$$\varepsilon_{ii} = \frac{\Delta l_i}{l_i^0}. \quad (6)$$

The potential 1.4 reproduces the bulk modulus of high-temperature γ -U. Results obtained for elastic constants and bulk modulus of α -U and pure Mo were within 20–40 % of the experimental values.

Table 3 – Elastic constants calculated for pure uranium and molybdenum. Corresponding relative deviations between calculated and experimental values are also presented.

	Experiment [15,17-20]	U-Mo-Xe 1.4 [dev]
Uranium		
B, α -U (300 K)	135.5	107 -21 %
C11	215	123.5 -42 %
C22	199	253 +27 %
C33	267	321 + 20 %
B, γ -U (~ 1100 K)	113.3	89 - 21 %
Molybdenum		
C11	450	585 + 30 %
C12	173	238 + 37 35 %

Thermal expansion of pure Mo

Next, the thermal expansion for pure Mo was calculated. The corresponding results are presented in Fig. 3. The potential for U-Mo-Xe 1.4 is in a good agreement with the experimental data [15] and with the dependence obtained previously with the potential developed for the binary Mo-Xe system [8].

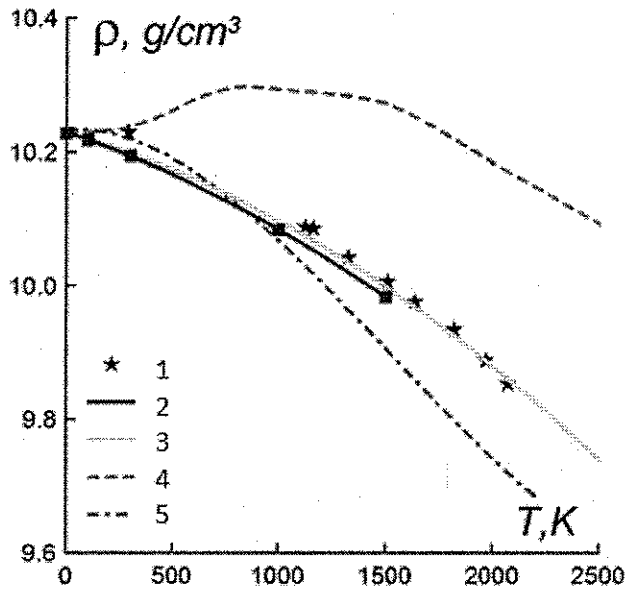


Figure 3 – Calculated thermal expansion of pure Mo. 1- experimental data [15]; 2 – results obtained in this work with the EAM potential U-Mo-Xe 1.4; 3 – EAM potential for Mo-Xe [8], 4 – EAM potential for Mo [21], 5 – calculations with the potential [22].

Room-temperature isotherms

Further, during verification we carried out a simulation of the uniform compression of pure Mo, Xe, and α -U at low temperatures to obtain the room temperature isotherms for each of these elements. It can be seen from Figs. 4 and 5 that in this case the potential 1.4 reproduces the experimental data with good accuracy. Results obtained for pure α -U (Fig. 6) were also consistent with the experimental ones.

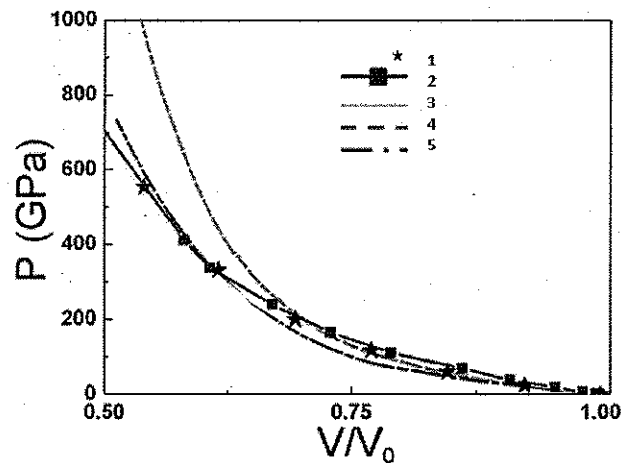


Figure 4 – Room temperature isotherm for pure Mo. 1 - existing experimental results [18]; 2 – isotherm calculated with the potential U-Mo-Xe 1.4; 3 – EAM potential for Mo-Xe [8]; 4 – EAM potential [21]; 5 – EAM potential developed in [22].

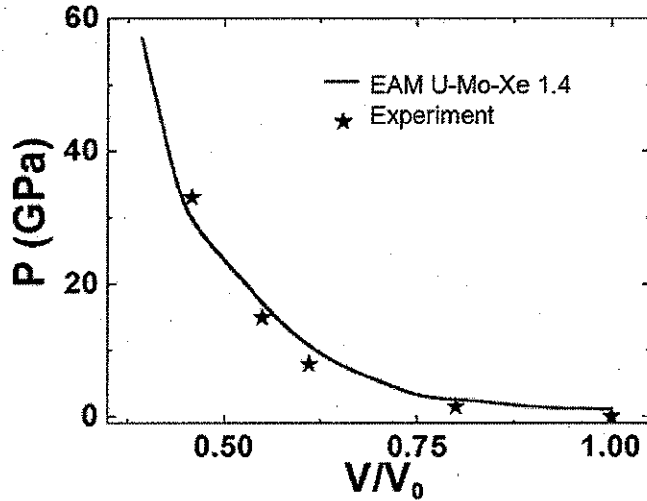


Figure 5 – Room temperature isotherm of pure Xe. Calculated results are presented in comparison with the experimental data [23].

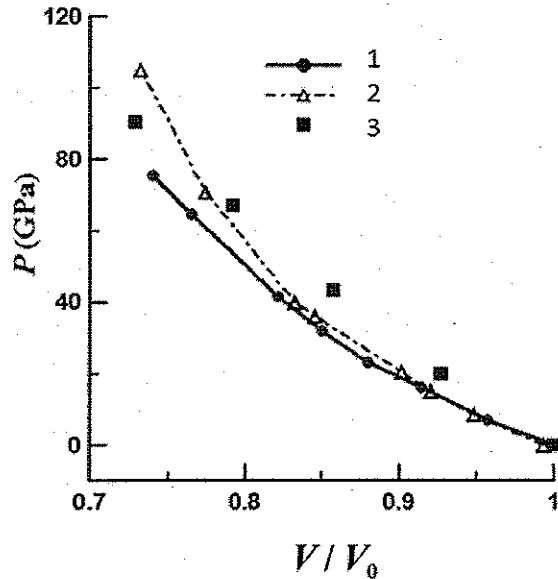


Figure 6 – Room temperature isotherm of low-temperature α -U phase. 1 - experimental DAC isotherm [17]; 2 - isotherm calculated with the EAM potential developed for pure uranium in [9]; 3 - potential U-Mo-Xe 1.4.

Melting temperatures

The potential 1.4 was used to calculate the phase transitions in pure molybdenum and uranium. Using a two-phase simulation technique [24, 25], we calculated the melting temperatures for pure Mo and pure U at zero pressure.

To calculate the melting temperature, we built a model of two coexisting phases with phase boundaries between liquid and bcc phase (a similar technique was used for U and for Mo). One

part of the box is filled by the atoms of metal in the bcc phase and another part by the liquid metal. In this way a model of the coexisting phases with the boundaries between the various phases is constructed. It is considered that at the melting temperature the boundary between bcc and liquid phases remains stable. Also at the melting temperature the time-temperature dependence was constant during the whole calculation time.

The results were compared with experiment, and the temperatures (with corresponding relative errors) are given in Table 4. We can see a little overestimation for U and underestimation for Mo.

Table 4 – Melting temperature of the pure components (U, Mo) at the $P \sim 0$ GPa

	Experiment	U-Mo-Xe 1.4 [dev.]
Mo	2890 K [26]	2690K -7 %
U	1406 K [14]	1530 K +9 %

Defect energies

The new potential for studying radiation defects generated by radiation of fission debris in U-Mo alloys can be used not only to verify the thermodynamical properties of U, Mo, and U-Mo but also to test how the potential obtained can reproduce defect properties.

At this time there is no reference information about the possible mechanisms of the defects formation and migration occurring exactly in U-Mo alloys. We therefore started the verification from a calculation of the defect formation energies in pure molybdenum and uranium.

Using the potential U-Mo-Xe 1.4, we calculated the self-interstitial atom (SIA) defect formation energies for pure molybdenum. The results were compared with the existing data. Formation energy of a single interstitial atom (SIA) can be determined as follows:

$$E_{SIA}^f = E_{(n+1)} - \frac{n+1}{n} E_n \quad (7)$$

where n is the number of atoms in the ideal structure, E_n is the energy of the ideal lattice, and E_{n+1} is the energy of the defect structure with one additional interstitial atom (we add a single uranium atom). To determine the values of E_n and E_{n+1} , we performed structure relaxation of the ideal and defect lattices. The results were compared with calculated SIA properties in various possible positions: dumbbell $\langle 100 \rangle$, dumbbell $\langle 110 \rangle$, dumbbell $\langle 111 \rangle$, crowdion $\langle 111 \rangle$, tetrahedral, and octahedral. For these computations the potential U-Mo-Xe 1.4 was used. In Fig. 7, one can see the difference between the C111 formation energy and the energies of formation of other possible interstitial defects in pure Mo. The potential 1.4 can describe the hierarchy of defect energies calculated within the DFT theory in [25,26]

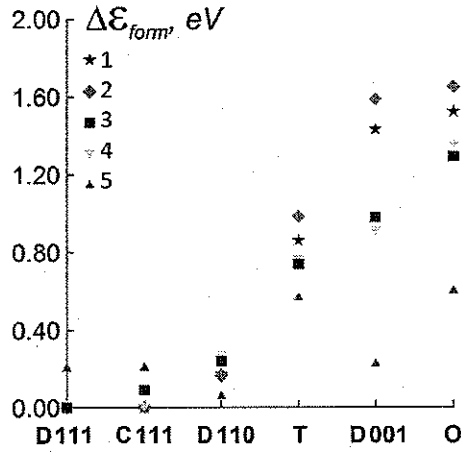


Figure 17 – Differences between defect formation energies for SIA in pure Mo. 1 – DFT [27]; 2 – DFT [28]; 3 – EAM U-Mo-Xe 1.4; 4 – EAM Mo-Xe [8]; 5 – EAM Mo [22].

Vacancy formation energy

During the investigation of the defects, MD simulations were performed to calculate vacancy formation energy:

$$E_{vac}^f = E_{(n-1)} - \frac{n-1}{n} E_n \quad (8)$$

The algorithm of the calculation was the same as for the SIA defects; that is, the energies of the ideal structure and the structure were compared with a single vacancy. According to expression (8), the values for a single vacancy formation energy were obtained in pure Mo (Table 5) and in pure bcc γ -U (Table 6). For γ -U, the structure relaxation procedure was corrected. We performed relaxation only for part of the simulation box, namely, for atoms that were situated at the distance less than 5.26 Å from the vacancy, in order to avoid deformation of the lattice occurring because of the high-temperature nature of the γ -U.

Table 5 – Single vacancy formation energy calculated for pure Mo (eV)

Experiment [29]	DFT [28]	EAM Mo-Xe[8]	EAM U-Mo-Xe 1.4
2.6 – 3.2	2.96	2.79	2.61

Table 6 – Single formation energy calculated for pure bcc γ -U (eV)

Experiment [30]	DFT [31]	EAM U [9]	EAM U-Mo-Xe 1.4
1.20 ± 0.25	1.08	1.52	2.246

The potential U-Mo-Xe 1.4 gives a good agreement with the experiment for vacancy formation in pure Mo, but it gives an incorrect, overestimated value for a single formation energy in pure bcc high-temperature uranium.

Conclusion

We developed several versions of the potential for the U-Mo-Xe system. The key point of this work was verification of these potentials by calculating some thermodynamical and mechanical properties of the U-Mo-Xe system and its components and further comparing the results with the existing experimental data and information obtained from DFT ab initio calculations. According to the results of the verification, the potential can reproduce the thermodynamical properties of U-Mo fuel alloys and pure U, Mo, and Xe. The potential U-Mo-Xe 1.4 was proved to reproduce a wide range of properties of pure elements with the most accuracy. Also, it allows one to calculate the properties of U-Mo alloys (computed lattice constants and thermal expansion compare well with the experimental data). The potential U-Mo-Xe 1.4 gives an adequate description of SIA defects in pure Mo because the initial reference structures for Mo include various types of defect structures.

To construct a reliable interatomic potential that would be applied directly to study defect properties in pure U and, further, in U-Mo alloys, we must add to the reference data the corresponding defect structures representing defect U and defect U-Mo lattices. The existing potential U-Mo-Xe 1.4 will be further modified to take this improvement into account. Also, this modification will help obtain better agreement with the vacancy formation energy for pure uranium.

It was shown that the potential gives good agreement with the experimental data for the lattice constants of U-Mo alloys, low-temperature α -U, high-temperature bcc γ -U, and molybdenum. The computed elastic and thermodynamical properties of U, Mo, and Xe were also consistent with the experimental results. Moreover, the potential enabled calculations of the thermal expansion coefficient for the U-Mo alloys and pure uranium and molybdenum and is applicable for investigation of the mechanisms of the radiation defects formation in U-Mo system and in pure U and Mo.

The results of the simulations performed allow the optimization of the structure of nuclear fuels for obtaining the required mechanical properties. The results of the MD computations will be useful for directing the experiments, for planning any modernization of nuclear systems, and for increasing their efficiency and safety.

Acknowledgments

This work was supported in part by the U.S. Department of Energy under Contract DE-AC02-06CH11357.

References

1. V. Sinha, G. Prasad, and P. Hegde, *J. of Alloys and Compounds*, 473, 238 (2009).
2. D. Burkes, R. Prabhakaram, and T. Hartmann, *J. Nuclear Engineering and design*, 240, 1332 (2010).

3. J. Rest, Y.S. Kim, G.L. Hofman, M.K. Meyer, and S.L. Hayes. U-Mo Fuels Handbook (Argonne National Laboratory, ANL-09/31), 2009.
4. B. A. Hilton, Review of oxidation rates of DOE spent nuclear fuel, Tech. Rep. (Argonne National Laboratory, 2000).
5. J. Rest, G. L. Hofman, Yeon Soo Kim, J. Nuclear Materials, 385, 563 (2009)
6. M. S. Daw and M. I. Baskes, Phys. Rev. B., 29, 6443 (1984).
7. F. Ercolessi and J. B. Adams, Europhys. Lett., 26, 583 (1994).
8. S.V. Starikov, Z. Insepov, J. Rest, A.Yu. Kuksin, G.E. Norman, V.V. Stegailov, and A.V. Yanilkin, Phys. Rev. B. (2011) to be published.
9. D.W. Smirnova, S.V. Starikov, and V.V. Stegailov, unpublished.
10. S. J. Plimpton, J. Comp. Phys., 117, 1 (1995).
11. G. Kresse and D. Joubert, Phys. Rev. B 59, 1758 (1999).
12. G. Kresse and J. Furthmuller, Phys. Rev. B 54, 11169 (1996).
13. P. Brommer and F. Gahler, Phil. Mag. 86, 753 (2006).
14. C.S Barrett, M.H. Mueller, and R.L. Hitterman, Phys. Rev. 129. № 2, 625-629 (1963).
15. J. W. Edwards, R. Speiser, and H. L. Johnston, J. App. Phys. 22, 424 (1951).
16. Y. Zhao, J. Zhang, D.W. Brown, D.R. Korzekwa, and R.S. Hixson, Phys. Rev. B 75. № 17. P. 174104 (2007)
17. C.S. Yoo, H. Cynn, and P. Soderlind, Phys. Rev. B. 57, no. 17, 10359 (1998).
18. Y. K. Vohra and A. L. Ruoff, Phys. Rev. B 42, 8651 (1990).
19. C. Taylor, Phys. Rev. B, 77, 094119 (2008).
20. F. H. Featherston and J. R. Neighbours, Phys. Rev. 130, 1324 (1963).
21. P. M. Derlet, D. Nguyen-Manh, and S. L. Dudarev, Phys. Rev. B 76, 054107 (2007).
22. M. W. Finnis and J. E. Sinclair, Philosophical Magazine A 50, 45 (1984).
23. V.D. Urlin, M.A. Mochalov, and O.L. Michailova, Matematicheskoe Modelirovanie 3, № 7. 1991.
24. J. R. Morris, C. Z. Wang, K. M. Ho, and C. T. Chan, Phys. Rev. B., 49, 3109 (1994).
25. S. Starikov and V. Stegailov, Phys. Rev. B 80, 22104 (2009).
26. D. Errandonea, B. Schwager, R. Ditz, C. Gessmann, R. Boehler, and M. Ross, Phys. Rev. B 63, 132104 (2001).
27. S. Han, L. A. Zepeda-Ruiz, G. J. Ackland, R. Car, and D. J. Srolovitz, Phys. Rev. B 66, 220101(R) (2002).
28. D. Nguyen-Manh, A. P. Horsfield, and S. L. Dudarev, Phys. Rev. B 73, 020101 (2006).
29. Landolt-Borstein Numerical Data and Functional Relationships in Science and Technology, Group III, vol. 25, Atomic Defects in Metals, ed. H. Ullmaier (Springer-Verlag, Berlin, 1991).
30. H. Matter, J. Winter, and W. Triftshauser, J. of Nucl. Mat., 88, 273 (1980).
31. S. Xiang, H. Huang, and L. Hsiung, J. of Nucl. Mat., 375, 113 (2008).